HHS Public Access

Author manuscript

Phys Med Biol. Author manuscript; available in PMC 2016 June 01.

Published in final edited form as:

Phys Med Biol. 2014 January 20; 59(2): 253–270. doi:10.1088/0031-9155/59/2/253.

Effects of Tissue Mechanical Properties on Susceptibility to Histotripsy-induced Tissue Damage

Eli Vlaisavljevich[1], **Yohan Kim**[1], **Gabe Owens**[1,2], **William Roberts**[1,3], **Charles Cain**[1], and **Zhen Xu**[1,2]

[1] Department of Biomedical Engineering, University of Michigan, Ann Arbor, MI

[2] Department of Pediatrics and Communicable Diseases, Division of Pediatric Cardiology, University of Michigan, Ann Arbor, MI

[3] Department of Urology, University of Michigan, Ann Arbor, MI

Abstract

Histotripsy is a non-invasive tissue ablation method capable of fractionating tissue by controlling acoustic cavitation. To determine the fractionation susceptibility of various tissues, we investigated histotripsy-induced damage on tissue phantoms and *ex vivo* tissues with different mechanical strengths. A histotripsy bubble cloud was formed at tissue phantom surfaces using 5-cycle long ultrasound pulses with peak negative pressure of 18 MPa and PRFs of 10, 100, and 1000 Hz. Results showed significantly smaller lesions were generated in tissue phantoms of higher mechanical strength. Histotripsy was also applied to 43 different *ex vivo* porcine tissues with a wide range of mechanical properties. Gross morphology demonstrated stronger tissues with higher ultimate stress, higher density, and lower water content were more resistant to histotripsy damage in comparison to weaker tissues. Based on these results, a self-limiting vessel-sparing treatment strategy was developed in an attempt to preserve major vessels while fractionating the surrounding target tissue. This strategy was tested in porcine liver *in vivo*. After treatment, major hepatic blood vessels and bile ducts remained intact within a completely fractionated liver volume. These results identify varying susceptibilities of tissues to histotripsy therapy and provide a rational basis to optimize histotripsy parameters for treatment of specific tissues.

Keywords

Histotripsy; Tissue Mechanical Properties; Vessel-sparing Ablation

Introduction

Histotripsy is a non-invasive tissue ablation method that controls acoustic cavitation to mechanically fractionate soft tissue through high pressure, microsecond-long ultrasound pulses at low duty cycles (<1%) (Kieran *et al.*, 2007; Parsons *et al.*, 2006a; Roberts *et al.*, 2006; Xu *et al.*, 2005b; Xu *et al.*, 2004). Histotripsy depends on the initiation and

Corresponding Author: Eli Vlaisavljevich Eli Vlaisavljevich, University of Michigan, Department of Biomedical Engineering, 2200 Bonisteel Blvd, Ann Arbor, MI 48109, USA. Phone: (734) 936-3674, ; Email: evlaisav@umich.edu

maintenance of a cavitation bubble cloud to produce tissue fractionation (Parsons *et al.*, 2007; Xu *et al.*, 2005a). With sufficiently high pressure and an adequate number of pulses, histotripsy can completely fractionate soft tissues into a liquefied acellular homogenate resulting in effective tissue removal (Hall *et al.*, 2007; Xu *et al.*, 2004). Histotripsy is currently being studied for many clinical applications where non-invasive tissue removal is desired including tissue debulking to treat benign prostatic hyperplasia (BPH) (Hempel *et al.*, 2011), thrombolysis (Maxwell *et al.*, 2009; Maxwell *et al.*, 2011), perforation of the atrial septum in the treatment of congenital heart diseases (Owens *et al.*, 2011; Xu *et al.*, 2010), tumor ablation (Styn *et al.*, 2010), kidney stone removal (Duryea *et al.*, 2011), and fetal interventions (Kim *et al.*, 2011; Kim *et al.*, 2013).

Tissue mechanical properties have been observed to affect the histotripsy process. The damage caused by histotripsy is often self-limiting at anatomical boundaries such as blood vessels, the capsule of an organ (e.g., the prostate), or fibrous structures (e.g., the collecting system in the kidney) (Lake *et al.*, 2008; Allam *et al.*, 2013; Styn *et al.*, 2011). The rate of histotripsy-induced tissue damage also seems to be affected by tissue mechanical properties, with a decreased efficiency for tissues with higher elastic modulus (Cooper *et al.*, 2004; Xu and Bigelow, 2011). Understanding the susceptibility of tissues with differing mechanical properties to histotripsy therapy will facilitate advancement of this technology. This knowledge will help improve parameter optimization strategies for current clinical applications and potentially identify new clinical targets.

In this work, we study how tissue mechanical properties impact the production and extent of damage caused by a histotripsy-induced bubble cloud. We hypothesize that increases in tissue mechanical strength will decrease the tissue's susceptibility to damage induced by histotripsy. To study the effect of mechanical properties on the tissue's susceptibility to histotripsy-induced damage without influences from changing bubble dynamics, a cavitating bubble cloud was generated in the same fluid (degassed water) at the tissue-fluid interface on tissue phantoms and *ex vivo* tissue. Erosion into the tissue surface was then analyzed. Mechanically tunable agarose tissue phantoms were used at varying mechanical properties. In addition, forty-three different types of *ex vivo* porcine tissues with a wide range of mechanical properties were also treated, and the production and extent of erosion were analyzed as a function of tissue properties including ultimate stress, ultimate fractional strain, density, and water content. These experiments will help determine the feasibility of using histotripsy as a method for non-invasive tissue removal in a wide range of potential clinical applications.

We also hypothesize that, based on the different susceptibilities of tissues to histotripsy, ablation of a target tissue can be self-limited at the boundaries of the vital anatomical structures if the vital structures are of higher mechanical strength (e.g. major blood vessels) than the target tissue volume (e.g. liver). The feasibility of a vessel-sparing ablation strategy was tested in porcine liver containing major hepatic vessels and bile ducts *in vivo*. As current thermal-based ablation methods have difficulty effectively ablating the tissue surrounding large vessels while preserving the vessels (Curley, 2001; Lu *et al.*, 2003; Marrero and Pelletier, 2006; Patterson *et al.*, 1998), such a vessel-sparing ablation feature can help histotripsy to address an important clinical need.

Materials and Methods

Therapeutic Ultrasound Treatment

Histotripsy pulses were generated by a 1 MHz focused ultrasonic transducer (Imasonic, SAS, Voray sur l'Ognon, France) with an aperture of 100 mm and focal length of 90 mm. Elements were driven in phase through a custom-designed class D amplifier with appropriate electrical matching circuits built in our laboratory and associated low voltage (20V DC power supply; E3630A Hewlett Packard Company, Palo Alto, CA, USA) and high voltage (600V DC power supply; GEN 600, TDK Lambda Americas Inc., San Diego, CA, USA) power supplies. Input signals were provided by a custom built Field-Programmable Gate Array (FPGA) board (Altera Corporation, San Jose, CA, USA) that functioned as a signal generator. Acoustic pressure waveforms produced by the 1 MHz therapeutic transducer were obtained using a fiber optic probe hydrophone built in house (Parsons *et al.*, 2006b). Pressure wave measurements were recorded in free-field in both degassed water and degassed 1,3-Butanediol (Sigma-Aldrich) at room temperature. Measurements were made in 1,3-Butanediol to prevent cavitation at the fiber tip at high pressures. The peak positive pressures were measured up to >80 MPa corresponding to a peak negative pressure of 15 MPa. At higher pressure, peak positive pressure could not be accurately measured due to instantaneous cavitation at the fiber tip in water and attenuation or saturation effects in Butanediol. The peak positive pressures corresponding to negative pressures >15 MPa that were used in these experiments are expected to be higher than 80 MPa.

Histotripsy Tissue Phantom Treatment

Agarose tissue phantoms with adjustable mechanical properties were used to provide a well-controlled environment for this study. The mechanical properties of agarose phantoms can be adjusted over a physiologically relevant range by changing agarose concentration. Agarose phantoms of 0.3%, 1%, 2.5%, and 5% w/v were selected to cover the mechanical strength of tissues found in the body from non-load bearing tissues such as fat, lung and brain to strong load bearing tissues such as tendon and cartilage (Normand *et al.*, 2000). For example, the ultimate stress of 5% agar gel is 214 kPa compared to 77.7 KPa for 2.5% gel while the compression moduli for 0.3%, 1%, 2.5%, and 5% agarose is 1.5 kPa, 38 kPa, 254 kPa, and 929 kPa, respectively (Normand *et al.*, 2000). These values cover the range of most soft tissues with moduli ranging from ~2-5 kPa (Lung, fat, heart) to ~900 kPa (cartilage). Agarose phantoms were prepared by slowly mixing agarose powder (Agarose Type VII, Sigma-Aldrich, St. Louis, MO, USA) into saline solution (0.9% sodium chloride, Hospira, Lake Forest, IL, USA) heated above 70°C. The solution was stirred on a hot plate until the gel became visually transparent. The agarose solution was then degassed under a partial vacuum of 20.5 psi for 30 minutes. After removing the agarose mixture from the vacuum, the solution was poured into rectangular polycarbonate tissue phantom holders and placed in a refrigerator at 4°C to allow gel to solidify prior to use.

A histotripsy bubble cloud was formed at the tissue phantom-water interface using 5-cycle long ultrasound pulses with peak negative pressure of 18 MPa and PRFs of 10, 100, and 1000 Hz (**Fig.1A**). These parameters were selected to ensure bubble cloud generation at the gel-water interface. Histotripsy treatments were applied to the agarose phantom surface at 6

locations each for 5,000 pulses. Erosion damage for each parameter was assessed by sectioning the tissue phantoms samples and measuring the maximum lesion depth and diameter using a microscope (Nikon Eclipse 50i, Nikon Corp., Tokyo, Japan). Statistical comparisons were made using a Student's t-test. P-values<0.05 were considered significant. Error bars on graphs represent standard error of the mean (SEM).

Histotripsy ex vivo Porcine Tissue Treatment

Forty-three types of excised porcine tissue of various mechanical properties were tested to cover the entire range of mechanical strength found in tissue. The tested samples included brain, heart (ventricular myocardium), fat, skeletal muscle, liver, lung, gallbladder, pancreas, kidney (cortex), spleen, stomach, lymph node, adrenal glands, thyroid, trachea, esophagus, bladder, skin, eye, optic nerve, femoral nerve, aorta, vena cava, femoral artery, femoral vein, ureter, urethra, ovary, uterus, cervix, small intestine, large intestine, tongue, articular cartilage, elastic cartilage, meniscus, ligament, tendon, heart valve tendons, trabecular bone, cortical bone, and tooth. The tissue samples were excised and immediately placed into degassed 0.9% saline solution and stored at 4°C. Prior to the experiments, the tissue was warmed to room temperature in degassed saline under a partial vacuum of 20.5 psi for 4 hours. Tissues thicker than the 10 mm axial size of the bubble cloud (muscle, liver, kidney, fat, lung, heart) were cut into 5 mm thick sections for treatment in order to assess for tissue perforation. All samples were used within 48 hours of harvesting.

The 1 MHz therapeutic ultrasound transducer was positioned in the water tank with the focus of transducer aligned to the tissue surface (**Fig.1A**). A histotripsy bubble cloud was formed at the tissue-water interface using 5-cycle long ultrasound pulses with peak negative pressure of 18 MPa and PRF of 1000 Hz. Bubble cloud formation and alignment were verified using high-speed optical and ultrasound imaging. Histotripsy treatments were applied to the tissue surface for 10 minutes (n=4). The longer treatment times for the *ex vivo* experiments were specifically chosen to demonstrate the resistance of stronger tissues wasn't merely a result of insufficient treatment time being required for stronger tissues, as the effects of histotripsy have been previously demonstrated to depend on the number of applied pulses. After treatment, the tissue samples were examined for damage (lesion formation) by gross morphology. Results were organized into tissues with complete erosion leading to perforation (large lesion through entire tissue), partial/little erosion (small observed lesions and/or some samples with no observed erosion), and no damage. Porcine tissue erosion results were further compared to tissue properties found in literature that have been correlated to tissue strength. In this work, ultimate stress, ultimate fractional strain, density, and water content values from literature were chosen as metrics for tissue properties. Ultimate stress and ultimate fractional strain were preferred to elastic modulus due to a more direct relevance to the investigation of tissue fractionation (properties at the point of rupture) as well as their wider availability and consistency within the literature. Density and water content values were used due to their high correlation to a wide range of mechanical properties (Diem K., 1970; Duck, 1990; ICRP, 1975; ICRU, 1989; Woodard and White, 1986). The average values of these tissue properties for the three groups (perforation, partial erosion, and no damage) were plotted as an average ± the standard deviation. Differences

between groups were compared using a Wilcoxon signed-rank t-test. P-values < 0.05 were considered significant.

In vivo Vessel-sparing Ablation

The feasibility of using histotripsy to selectively ablate porcine liver while preserving blood vessels of higher mechanical strength was investigated *in vivo*. The livers of two pigs (94 and 66 lbs.) were treated with histotripsy. Porcine liver was chosen due to the anatomical structures including hepatic blood vessels and bile ducts present within the organ. Liver vasculature covers a wide range of sizes and mechanical properties from large hepatic vessels, which reach 1.5 cm in diameter and ultimate stresses of 1-3 MPa down to small vessels and capillaries <10 μm in diameter with negligible mechanical strength (Fratzl, 2008; Holzapfel and Ogden, 2003; Marieb and Hoehn, 2007). In comparison, the ultimate stress of liver is 0.27 MPa (Moffitt *et al.*, 2002). Pigs were pre-medicated with Telazol (6 mg/kg) and Xylazine (2.2 mg/kg) and an intravenous catheter was placed in an auricular vein. Pigs underwent endotracheal intubation and were maintained under full anesthesia on isoflurane gas (1.5-2.0%) for the duration of the procedure. Anesthetized pigs were placed in a dorsal recumbent position upon the surgical table and the skin over the targeted tissue was treated with a depilatory cream to remove hair to improve ultrasound coupling. To ensure ultrasound propagation to targeted tissue, a degassed water bolus was coupled to the skin with a thin plastic membrane and ultrasound coupling gel.

An 8 MHz phased array ultrasonic imaging probe (Model S8, Philips Electronics, Andover, MA) was aligned coaxially with the therapy transducer. An ultrasound imaging system (Sonos 7500, Philips Electronics, Andover, MA) was used to locate the liver target and histotripsy was applied transcutaneously through the ribs and overlying tissue **(Fig.1B)**. The cavitation cloud was initiated by slowly increasing the driving voltage until a bubble cloud was visualized in the liver on ultrasound imaging. Histotripsy (10 cycles, 500 Hz PRF, estimated *in situ* peak negative pressure ~17 MPa) was applied to liver and the therapy focus was mechanically scanned over 12 cm^3 (3×2×2 cm scan) and 18 cm^3 (3×3×2 cm scan) volumes, resulting in significantly larger actual treated regions due to the size of the bubble cloud and breathing motion. Each point within the block was treated for 4 seconds (2,000 pulses) and adjacent treatment spots were separated by 2 mm in the transverse plane and by 5 mm axially. The *in vivo* parameters were chosen based on previous experiments demonstrating that the liver can be completely fractionated within 2,000 pulses. The pulse duration of 10 cycles was used here to keep consistent with previous *in vivo* liver ablation experiments. Doppler images of large blood vessels within the treatment region were taken before and after treatment to determine whether vessels continued to have blood flow. After the procedure, the pigs were euthanized without recovery with an intravenous injection of sodium pentobarbital (140-160 mg/kg) and the liver was harvested and imaged with a 7T small animal MRI scanner (Varian, Inc., Palo Alto, CA, USA). Both T1 and T2 weighted multi-slice spin-echo images of the liver were acquired along both coronal and axial planes.

After the MRI procedure, the liver was fixed in formalin and dissected, with samples stained with hematoxylin and eosin (H&E). The damage to the liver, vessels, and bile ducts within and surrounding the treatment region was examined histologically under a microscope

(Nikon Eclipse 50i) using 4x, 10x, 20x, and 40x objective lenses. To quantitatively assess the distribution of blood vessels remaining after histotripsy, the number of vessels was counted using three H&E slides for each lesion (total n=6). Vessels were organized into seven groups based on the type of vessel and size (inner diameter): large arteries (>1 mm), large veins (>1 mm), small arteries (0.3-1 mm), small veins (0.1-1 mm), arterioles (20-300 μm), venules (20-100 μm), and capillaries (<10 μm). The thickness of the intima, media, and adventitia was included for each vessel type, as the mechanical strength of the blood vessels is dependent on the thickness of these layers (Duck, 1990; Fratzl, 2008; Holzapfel and Ogden, 2003; Marieb and Hoehn, 2007; Schulze-Bauer *et al.*, 2002; Yamada, 1973). The media and adventitial layers are primarily responsible for vessel mechanical strength under normal physiologic conditions (Fratzl, 2008; Holzapfel and Ogden, 2003; Schulze-Bauer *et al.*, 2002). The loosely woven collagen fibers in the adventitial layer align under loading conditions to provide the vessel with a high ultimate stress necessary to prevent over-distension and vessel rupture (Fratzl, 2008; Holzapfel and Ogden, 2003; Schulze-Bauer *et al.*, 2002). Although quantitative values of mechanical strength could not be found for all the different vessel groups, increasing thickness of the media and adventitia indicates higher mechanical strength. For each H&E slide, the number of vessels of each type in one hundred 1 mm^2 regions of the lesion and surrounding liver (control) was counted. The mean and standard deviation of the number of vessels for the six slides were calculated with the lesion results plotted as a percentage of the control region. To compare the treatment and control regions, a two-sided Student's t-test was conducted for each vessel type between lesion and controls (n=6). P-values <0.05 were considered statistically significant. All procedures used in this work were reviewed and approved by the University Committee on Use and Care of Animals at the University of Michigan.

Results

Histotripsy in Agarose Tissue Phantom

The diameter and depth of lesions decreased for tissue phantoms with higher agarose concentration, which also had higher mechanical strength (**Fig.2**). The compression moduli of the agarose gels increases with concentration from 1.5 kPa, 38 kPa, 254 kPa, and 929 kPa for 0.3%, 1%, 2.5%, and 5% agarose, respectively. A statistically significant decrease in the mean maximum diameter of the lesion was observed for tissue phantoms of increased strength treated at all PRFs with larger differences between the 1%, 2.5%, and 5% tissue phantoms and smaller decreases between the 0.3% and 1% samples (**Fig.2A**). For example, at a PRF of 10 Hz, the mean of the maximum diameter of the lesion decreased from 3.95 mm for the 0.3% gel to 3.56 mm for the 1% gel, 2.84 mm for the 2.5% gel, and 0.87 mm for the 5% gel. Similarly, a statistically significant decrease in the maximum lesion depth was observed for higher agarose concentration phantoms. Larger differences were again seen between the 1%, 2.5%, and 5% tissue phantoms (**Fig.2B**). For example, at a PRF of 10 Hz, the maximum depth decreased from 9.61 mm for the 0.3% gel to 9.47 mm for the 1% gel, 7.21 mm for the 2.5% gel, and 4.30 mm for the 5% gel. All decreases in lesion depth and diameter were statistically significant ($p<0.05$) except between the 0.3% and 1% gels at 100 Hz PRF (depth: 9.52 mm, 9.1 mm, p=0.08; diameter: 3.52 mm, 3.41 mm, p=0.12). The lesion size in the lower concentration agarose gels (0.3% and 1%) closely matched the

bubble cloud size in free field of approximately 3.5 mm in the transversal plane and 10 mm in the axial plane. Additionally, the results show a decrease in maximum diameter and depth with increasing PRF treatments (**Fig.2**). For example for the 2.5% agarose phantom, the maximum lesion diameters were 2.82±0.18 mm, 2.36±0.21 mm, and 1.26±0.10 mm, and the maximum lesion depths were 7.21±0.24 mm, 6.23±0.42 mm, and 5.11±0.19 mm for PRFs of 10, 100, and 1000 Hz, respectively.

Histotripsy in ex vivo Porcine Tissue

Histotripsy-induced erosion was examined using 43 types of harvested porcine tissues (n=4) from non-load bearing tissues such as fat, lung and brain to strong load bearing tissues such as tendon and cartilage. All tissues were exposed to a cavitating histotripsy bubble cloud for 10 minutes generated using 5-cycle pulses at 18 MPa peak negative pressure and 1 kHz PRF. Gross morphology demonstrated complete erosion leading to perforation in the majority of soft tissues tested including brain, heart, fat, skeletal muscle, liver, lung, gallbladder, pancreas, kidney, spleen, stomach, lymph node, adrenal glands, thyroid, esophagus, eye, optic nerve, femoral nerve, ureter, urethra, ovary, ovarian cyst, uterus, cervix, small intestine, large intestine, and ligament (**Fig.3)**. A smaller group of tissues treated with histotripsy showed no sign of damage, including skin, cartilage (all types), tendon, heart valve tendons, trabecular bone, cortical bone, and tooth, demonstrating certain tissues are less susceptible to histotripsy induced damage (**Fig.4**). Additionally, partial erosion was observed in some tissues including tongue (small lesion), bladder (small lesion), urethra (damage to inner lining, no damage to outer layer), and blood vessels (damage to intima and media, no damage to adventitia) (**Fig.4**). The entire list of erosion results are recorded in **Table 1**. Edema at the therapy target was observed for intestines, pancreas, thyroid, and gallbladder **(Table 1)**. All tissues with observed edema also exhibited complete erosion.

Tissue erosion results were compared to tissue ultimate stress, ultimate fractional strain, density, and water content values (**Table 2**). Results demonstrated a statistically significant difference in average tissue strength between perforated tissues compared to the undamaged group, with perforated tissues having a lower average density, higher average water content, lower ultimate stress, and higher ultimate fractional strain (**Fig.5**). The average density of perforated tissues of 1040.4±32.5 kg/m^3 was lower than the density of undamaged tissues of 1509.7±488.3 kg/m^3 ($p<0.05$) (**Fig.5**). The average water content for perforated tissues of 76.1±5.9% was higher ($p<0.05$) than the average water content in undamaged tissues of 43.7±27.2% (**Fig.5B**). The average ultimate tensile stress for perforated tissues was 0.3525±. 26 MPa compared to an average of 40.44±55.80 MPa for undamaged tissues (**Fig.5C**). All tissues with ultimate stresses below 1 MPa were completely eroded with the only exception being the partial damage to the bladder which had an extremely high ultimate fractional strain (**Table 1**). Ultimate fractional strain showed a statistically significant difference ($p<0.05$) between completely perforated tissues which had an average ultimate strain of 0.8163±0.36 compared to 0.2348±0.26 for undamaged tissues (**Fig.5D**). No statistically significant differences were observed between perforated and partially damaged groups for any of the tissue properties compared. The complete list of erosion results with corresponding tissue properties are recorded in **Table 2**.

In vivo Vessel-sparing Ablation

Two intact porcine livers containing a hierarchy of blood vessels were treated *in vivo* using histotripsy with a peak negative pressure right above the threshold to initiate a bubble cloud in the liver based on the ultrasound imaging feedback. Our *ex vivo* experiments showed a higher resistance of vessels to histotripsy-induced erosion in comparison to liver tissue. MRI multi-slice analysis of the *in vivo* lesions demonstrated lesion volumes of approximately 18 cm^3 and 60 cm^3 with multiple large vessels remaining within the fractionated liver volumes (**Fig.6A**). Large hepatic vessels visible within the lesion were shown to remain patent on ultrasound Doppler imaging **(Fig.6B-C)**. Histological evaluation of the lesion indicated hepatic parenchyma was completely fractionated into acellular debris while large vessels (>1 mm diameter) remained intact within the treated region. No damage or perforation to any vessels larger than 1mm in diameter was observed. In the *ex vivo* study, partial damage was observed to the intima and media of large vessels while the adventitia remained intact. However, for those experiments, histotripsy was applied directly to a stretched open *ex vivo* vessel wall and treated for much longer treatment times (10,000 pulses). The extensive connective tissue observed to surround the large hepatic vessels in the adventitial layer *in vivo* likely enhanced the vessel resistance to histotripsy and prevented the bubbles from damaging the weaker media and intima layers. No damage to the endothelial layer was observed for vessels that remained completely intact within the treated volume. An extensive network of intermediate vessels (300-1000 μm diameter) and bile ducts was also found intact throughout the treated lesion **(Fig.7)**. Localized hemorrhage was visible within the histotripsy lesion due to the rupture of capillaries and small vessels.

Quantitative analysis of vessels remaining inside the lesions showed a statistically significant decrease ($p<0.05$) in the number of capillaries, venules, arterioles, and small veins compared to intact liver controls (**Fig.8**). The lesions contained 64.9% of small veins, 13.9% of arterioles, and 3.9% of venules compared to controls while no capillaries were observed inside the lesion. No statistically significant difference ($p>0.05$) was found for large arteries, large veins, or small arteries with 105.5% of large arteries, 110% of large veins, and 78.5% of small arteries remaining compared to controls (**Fig.8**). The blood vessel types remaining inside the treated region had larger inner diameters and thicker walls with thicker media and adventitial layers than the vessel types ablated by histotripsy (**Fig.8**) (Duck, 1990; Jain, 1988; Marieb and Hoehn, 2007; Yamada, 1973). For example, the thickness of the adventitial layer was between 200-400 μm for the larger arteries, 60-300 μm for larger veins, 20-200 μm for smaller arteries, 6-120 μm for smaller veins, and < 20 μm for arterioles and venules. Thicker media and adventitial layers have previously been correlated with increases in vessel mechanical strength with adventitial layers of 200-400 μm associated with an ultimate tensile stress >1MPa for large vessels which is higher than the ultimate stress of liver (0.27 MPa) (Duck, 1990; Jain, 1988; Marieb and Hoehn, 2007; Yamada, 1973; Fratzl, 2008; Holzapfel and Ogden, 2003; Schulze-Bauer *et al.*, 2002). These results indicate that vessels with increased mechanical strength were preserved inside the histotripsy lesion while smaller, weaker vessels were ablated along with the liver.

Discussion

In this study, the effectiveness of histotripsy in treating tissues of varied mechanical characteristics was investigated. Results show a decrease in susceptibility to histotripsy damage for tissues of increased mechanical strength. The wide range of tissues tested in this work provides a guide to the feasibility of using histotripsy to address a variety of clinical applications in which the removal of a specific tissue type is desired. Additionally, the *in vivo* feasibility of using histotripsy for vessel-sparing ablation was investigated, suggesting histotripsy has the potential to act as a self-limiting tissue-selective fractionation technique.

For both tissue phantom and *ex vivo* tissue experiments, the cavitating bubble cloud was generated at the tissue-fluid interface in the degassed water using the same acoustic pressure. Similar levels of bubble expansion and collapse were expected to be produced in the degassed water for treatment of different samples, but tissues with higher mechanical strength displayed higher resistance to the damage generation. These results suggest that stronger tissues can resist more of the mechanical loading from the cavitation activity before mechanical breakdown induced by histotripsy occurs. Results demonstrated that undamaged tissues had higher average densities, lower average water content, higher ultimate stress, and lower ultimate fractional strain than the tissues perforated by histotripsy. The finding that undamaged tissues had a higher ultimate stress makes sense intuitively as tissues with higher ultimate stress are by definition more resistant to fractionation. The finding that undamaged tissues had lower ultimate strains, however, suggests that tissue resistance to deformation (high ultimate stress) appears to play a more significant role in resisting histotripsy-induced damage than withstanding large deformations (high ultimate strain) for the majority of tissues. The only tissue with a low ultimate stress observed to resist erosion was the urinary bladder, which was only partially eroded (very small lesion formed only partially through tissue). However, the bladder had a higher ultimate fractional strain (2.26) than all other tissues, which allows the bladder to undergo large mechanical strains without rupture. This finding suggests a different method of resisting histotripsy damage for the bladder compared to the other undamaged tissues.

This study showed that, given the same cavitation activity at a tissue-fluid interface, tissues with higher mechanical strength were more resistant to the damage induced by histotripsy. For bulk tissue fractionation, the bubble expansion is impeded in stiffer tissue resulting in less cavitation effects on the tissue in addition to the increased resistance of stronger tissues to histotripsy-induced damage. This impeded bubble expansion will likely result in an even higher damage threshold for bulk fractionation of stronger tissues. One way to potentially work around the impeded bubble expansion in stronger tissues may be to create a fluid-tissue interface in the bulk tissue by generating a fluid homogenate in the bulk tissue and erode outward from there (similar to the blood vessels in the *in vivo* situation in this study), which may be an effective approach to fractionation stiff bulk tissue. Future work will study the nonlinear viscoelastic response of tissues under the high strain rates induced by histotripsy to provide a more complete understanding of the results of this study in order to develop optimal strategies to fractionate tissues with different mechanical properties for both tissue erosion and bulk fractionation. Future studies will also investigate the specific mechanism with which histotripsy damages tissues and the process with which stronger

tissues are capable of resisting histotripsy on the micro-scale (i.e. effects of extracellular matrix and cytoskeletal mechanics).

In addition to erosion, edema was observed in the pancreas, small and large intestines, thyroid, and gallbladder. This fluid uptake was observed for tissue adjacent to the eroded lesion with the extent of fluid uptake being most noticeable in the pancreas. Fluid uptake into tissue during cavitation has been previously observed for uterine endometrium and is possibly due to the cavitation cloud pumping fluid across the tissue boundary via microjetting (Lin *et al.*, 2010). Edema was not observed in uterine tissue in this study, likely because treatment was applied to the external uterine perimetrium rather than the endometrium. The tissues in which edema was observed in this work have similar structure to uterine endometrium, i.e. membranous tissue structures with large surface area. This finding suggests that the fluid uptake phenomenon is most likely to occur in membranous tissues with high surface area commonly found in digestive system organs or glandular structures. In addition to asymmetric bubble collapse and microjetting, it is also possible that the observed fluid uptake into these tissues is a result of ultrasonic atomization and fountain formation which has been observed in studies of boiling histotripsy (Simon *et al.*, 2012; Wang *et al.*, 2013), as well as possible fluid uptake caused by acoustic streaming from the histotripsy bubble cloud which has been shown to generate high velocity fluid flows (Park *et al.*, 2013). Future work will be needed to investigate the specific mechanism causing fluid uptake.

The feasibility of using histotripsy as a vessel-sparing selective fractionation technique was shown *in vivo*. Based on the results of *ex vivo* experiments where the large vessels had a higher resistance to histotripsy-induced damage than liver, we hypothesized that by selecting an appropriate pressure and treatment time, fractionation of the liver could be self-limiting at the boundaries of large vessels. Results supported our hypothesis demonstrating no statistically significant difference in the number of large arteries and veins remaining inside the histotripsy treated lesion compared to intact liver. The vessel preservation is highly dependent on vessel size and structure. While large vessels were preserved, there was a statistically significant decrease in the number of smaller vessels remaining inside the lesion. The high ultimate stress or high ultimate strain of large vessels could both play a role in the preservation of these vessels, which are highly compliant under normal physiologic conditions but also have a high ultimate stress under loading conditions due to the fibrous connective tissue in the adventitial layer. It is likely that the number and type of vessels remaining inside the histotripsy lesions would change based on treatment parameters. For example, increasing the pressure or number of pulses may result in fewer small arteries and veins remaining after treatment while very long treatment times could potentially rupture the major blood vessels.

An interesting observation from the *ex vivo* experiments performed in this work was that the femoral nerve was completely fractionated while a previous study demonstrated histotripsy spared nerves during treatment for BPH (Styn *et al.*, 2011). The mechanical properties of the femoral nerve are closely related to the other perforated tissues and are in agreement with our hypothesis that softer tissues are more susceptible to histotripsy damage. There are two possible explanations to account for the discrepancy with the previous study in the prostate.

First, the *ex vivo* treatments performed in this work consisted of many more pulses than what was applied to the prostate in the paper by Styn et al. Second, it is likely that the nerve-sparing response previously observed is aided by the connective tissue surrounding nerves *in vivo* in a similar way in which the adventitial layer appears to protect the blood vessels from histotripsy induced damage. The nerves treated in this study were harvested without the surrounding connective tissue in order to see the effects of histotripsy on only the nerve tissue itself, which could explain why the nerve was perforated by histotripsy in this study while previously being preserved *in vivo*. Future work will further investigate the potential of nerve-sparing tissue fractionation and the role of the surrounding connective tissue in the process.

In addition to the increased resistance to histotripsy, separate work has demonstrated increases in the cavitation initiation threshold in stronger tissues, which likely plays a role in the selective ablation technique (Vlaisavljevich *et al.*, 2011). The level of bubble expansion also decreased in tissue with higher mechanical strength (Vlaisavljevich *et al.*, 2011). These effects act complementary to one another and suggest the ability to further optimize this approach to utilize both the cavitation threshold gradient as well as the damage resistance gradient. Future work will aim to optimize this self-limiting vessel-sparing fractionation technique and expand it to other critical tissues with higher mechanical strength, such as major nerves or collecting systems. This approach can be beneficial for clinical applications where removal of a tissue surrounding important anatomical structures is desired, such as the removal of tumors near large vessels which is currently a major problem for surgery and thermal ablation therapies which have difficulty effectively ablating tissue surrounding large vessels while preserving the vessels (Curley, 2001; Lu *et al.*, 2003; Marrero and Pelletier, 2006; Patterson *et al.*, 1998).

Summary

In this study, the effects of tissue properties on histotripsy tissue damage were investigated. The results of this work demonstrate decreased or no fractionation for tissues of increased mechanical strength. Additionally, the feasibility of using histotripsy as a tissue selective ablation method was demonstrated in an *in vivo* porcine liver where large hepatic vessels with higher mechanical strength were preserved while surrounding hepatic parenchyma with lower mechanical strength was completely fractionated. These results improve our understanding of how tissue mechanical properties affect histotripsy and provide a rational basis to extend histotripsy to address additional clinical needs.

Acknowledgements

The authors would like to thank Dr. Kimberly Ives for her help with porcine tissue experiments and Mr. Steven Allen for his help with MRI imaging of liver lesions. This material is based upon work supported by the National Science Foundation Graduate Research Fellowship. This work was supported by grants from National Institute of Health (R01 EB008998 and R01 CA134579), a Research Scholar Grant, RSG-13-101-01-CCE from the American Cancer Society, and The Hartwell Foundation. Disclosure notice: Drs. William W. Roberts, Charles A. Cain, and Zhen Xu have financial interests and/or other relationship with HistoSonics Inc.

References

Allam C, Wilkinson JE, Cheng X, Ives K, Hall TL, Roberts WW. Histotripsy Effects on the Bladder Trigone: Functional and Histologic Consequences in the Canine Model. J Endourol. 2013

Cooper M, Xu Z, Rothman E, Levin A, Advincula A, Fowlkes JB, Cain C. Controlled Ultrasound Tissue Erosion: the Effects of Tissue Type, Exposure Parameters, and the Role of Dynamic Microbubble Activity. IEEE International Ultrasonics, Ferroelectric, and Frequency Control Joint 50th Anniversary Conference. 2004:1808–11.

Curley SA. Radiofrequency ablation of malignant liver tumors. Oncologist. 2001; 6:14–23. [PubMed: 11161225]

Diem, KLC. Documenta Geigy scientific tables. 7th Edition.. Macclesfield; 1970.

Duck, FA. Physical properties of tissue: a comprehensive reference book. Academic Press; 1990.

Duryea AP, Hall TL, Maxwell AD, Xu Z, Cain CA, Roberts WW. Histotripsy erosion of model urinary calculi. J Endourol. 2011; 25:341–4. [PubMed: 21091223]

Fratzl, P. Collagen: Structure and Mechanics. Springer Science+Business Media, LLC; New York, NY: 2008.

Hall TL, Kieran K, Ives K, Fowlkes JB, Cain CA, Roberts WW. Histotripsy of rabbit renal tissue in vivo: temporal histologic trends. J Endourol. 2007; 21:1159–66. [PubMed: 17949317]

Hempel CR, Hall TL, Cain CA, Fowlkes JB, Xu Z, Roberts WW. Histotripsy fractionation of prostate tissue: local effects and systemic response in a canine model. J Urol. 2011; 185:1484–9. [PubMed: 21334667]

Holzapfel, GA.; Ogden, RW. Biomechanics of Soft Tissue in Cardiovascular Systems. Springer-Verlag; New York, NY: 2003.

ICRP. Report of the Task Group on Reference Man : a report. Pergamon Press; Oxford, New York: 1975.

ICRU. Tissue Substitutes in Radiation Dosimetry and Measurement. Intl Commission on Radiation; 1989.

Jain RK. Determinants of tumor blood flow: a review. Cancer Res. 1988; 48:2641–58.

Kieran K, Hall TL, Parsons JE, Wolf JS Jr. Fowlkes JB, Cain CA, Roberts WW. Refining histotripsy: defining the parameter space for the creation of nonthermal lesions with high intensity, pulsed focused ultrasound of the in vitro kidney. J Urol. 2007; 178:672–6. [PubMed: 17574617]

Kim Y, Fifer CG, Gelehrter SK, Owens GE, Berman DR, Vlaisavljevich E, Allen SP, Ladino-Torres MF, Xu Z. Developmental impact and lesion maturation of histotripsy-mediated non-invasive tissue ablation in a fetal sheep model Ultrasound. Med Biol. 2013; 39:1047–55.

Kim Y, Gelehrter SK, Fifer CG, Lu JC, Owens GE, Berman DR, Williams J, Wilkinson JE, Ives KA, Xu Z. Non-invasive pulsed cavitational ultrasound for fetal tissue ablation: feasibility study in a fetal sheep model. Ultrasound Obstet Gynecol. 2011; 37:450–7. [PubMed: 21433165]

Lake AM, Xu Z, Wilkinson JE, Cain CA, Roberts WW. Renal ablation by histotripsy--does it spare the collecting system? J Urol. 2008; 179:1150–4. [PubMed: 18206166]

Lin, KW.; Shao, X.; Xu, Z.; Fowlkes, JB.; Cain, C. Ultrasound-induced fluid uptake phenomenon in porcine uterine tissue.. IEEE International Ultrasonics Symposium; San Diego, CA. 2010.

Lu DS, Raman SS, Limanond P, Aziz D, Economou J, Busuttil R, Sayre J. Influence of large peritumoral vessels on outcome of radiofrequency ablation of liver tumors. J Vasc Interv Radiol. 2003; 14:1267–74. [PubMed: 14551273]

Marieb, EN.; Hoehn, K. Human Anatomy and Physiology. 7th Edition. Pearson Education, Inc.; 2007.

Marrero JA, Pelletier S. Hepatocellular carcinoma. Clin Liver Dis. 2006; 10:339–51. ix. [PubMed: 16971265]

Maxwell AD, Cain CA, Duryea AP, Yuan L, Gurm HS, Xu Z. Noninvasive thrombolysis using pulsed ultrasound cavitation therapy - histotripsy Ultrasound. Med Biol. 2009; 35:1982–94.

Maxwell AD, Owens G, Gurm HS, Ives K, Myers DD Jr. Xu Z. Noninvasive treatment of deep venous thrombosis using pulsed ultrasound cavitation therapy (histotripsy) in a porcine model. J Vasc Interv Radiol. 2011; 22:369–77. [PubMed: 21194969]

Moffitt TP, Baker DA, Kirkpatrick SJ, Prahl SA. Mechanical properties of coagulated albumin and failure mechanisms of liver repaired with the use of an argon-beam coagulator with albumin. J Biomed Mater Res. 2002; 63:722–8. [PubMed: 12418016]

Normand V, Lootens DL, Amici E, Plucknett KP, Aymard P. New insight into agarose gel mechanical properties. Biomacromolecules. 2000; 1:730–8. [PubMed: 11710204]

Owens GE, Miller RM, Ensing G, Ives K, Gordon D, Ludomirsky A, Xu Z. Therapeutic ultrasound to noninvasively create intracardiac communications in an intact animal model. Catheter Cardiovasc Interv. 2011; 77:580–8. [PubMed: 20853366]

Park S, Maxwell AD, Owens GE, Gurm HS, Cain CA, Xu Z. Non-invasive embolus trap using histotripsy-an acoustic parameter study. Ultrasound Med Biol. 2013; 39:611–9. [PubMed: 23415285]

Parsons JE, Cain CA, Abrams GD, Fowlkes JB. Pulsed cavitational ultrasound therapy for controlled tissue homogenization. Ultrasound Med Biol. 2006a; 32:115–29. [PubMed: 16364803]

Parsons JE, Cain CA, Fowlkes JB. Cost-effective assembly of a basic fiber-optic hydrophone for measurement of high-amplitude therapeutic ultrasound fields. J Acoust Soc Am. 2006b; 119:1432–40. [PubMed: 16583887]

Parsons JE, Cain CA, Fowlkes JB. Spatial variability in acoustic backscatter as an indicator of tissue homogenate production in pulsed cavitational ultrasound therapy. IEEE Trans Ultrason Ferroelectr Freq Control. 2007; 54:576–90. [PubMed: 17375826]

Patterson EJ, Scudamore CH, Owen DA, Nagy AG, Buczkowski AK. Radiofrequency ablation of porcine liver in vivo: effects of blood flow and treatment time on lesion size. Ann Surg. 1998; 227:559–65. [PubMed: 9563546]

Roberts WW, Hall TL, Ives K, Wolf JS Jr. Fowlkes JB, Cain CA. Pulsed cavitational ultrasound: a noninvasive technology for controlled tissue ablation (histotripsy) in the rabbit kidney. J Urol. 2006; 175:734–8. [PubMed: 16407041]

Schulze-Bauer CA, Regitnig P, Holzapfel GA. Mechanics of the human femoral adventitia including the high-pressure response. Am J Physiol Heart Circ Physiol. 2002; 282:H2427–40. [PubMed: 12003855]

Simon JC, Sapozhnikov OA, Khokhlova VA, Wang YN, Crum LA, Bailey MR. Ultrasonic atomization of tissue and its role in tissue fractionation by high intensity focused ultrasound. Phys Med Biol. 2012; 57:8061–78. [PubMed: 23159812]

Styn N, Hall TL, Fowlkes JB, Cain CA, Roberts WW. Histotripsy homogenization of the prostate: thresholds for cavitation damage of periprostatic structures. J Endourol. 2011; 25:1531–5. [PubMed: 21815807]

Styn NR, Wheat JC, Hall TL, Roberts WW. Histotripsy of VX-2 tumor implanted in a renal rabbit model. J Endourol. 2010; 24:1145–50. [PubMed: 20575696]

Vlaisavljevich E, Cain CA, Xu Z. Effects of Tissue Mechanical Properties on Histotripsy. IEEE International Ultrasonics Symposium. 2011

Wang YN, Khokhlova T, Bailey M, Hwang JH, Khokhlova V. Histological and biochemical analysis of mechanical and thermal bioeffects in boiling histotripsy lesions induced by high intensity focused ultrasound. Ultrasound Med Biol. 2013; 39:424–38. [PubMed: 23312958]

Woodard HQ, White DR. The composition of body tissues. Br J Radiol. 1986; 59:1209–18. [PubMed: 3801800]

Xu J, Bigelow TA. Experimental investigation of the effect of stiffness, exposure time and scan direction on the dimension of ultrasound histotripsy lesions. Ultrasound Med Biol. 2011; 37:1865–73. [PubMed: 21963031]

Xu Z, Fowlkes JB, Ludomirsky A, Cain CA. Investigation of intensity thresholds for ultrasound tissue erosion. Ultrasound Med Biol. 2005a; 31:1673–82. [PubMed: 16344129]

Xu Z, Fowlkes JB, Rothman ED, Levin AM, Cain CA. Controlled ultrasound tissue erosion: the role of dynamic interaction between insonation and microbubble activity. J Acoust Soc Am. 2005b; 117:424–35. [PubMed: 15704435]

Xu Z, Ludomirsky A, Eun LY, Hall TL, Tran BC, Fowlkes JB, Cain CA. Controlled ultrasound tissue erosion. IEEE Trans Ultrason Ferroelectr Freq Control. 2004; 51:726–36. [PubMed: 15244286]

Xu Z, Owens G, Gordon D, Cain C, Ludomirsky A. Noninvasive creation of an atrial septal defect by histotripsy in a canine model. Circulation. 2010; 121:742–9. [PubMed: 20124126]

Yamada, H. Strength of biologic materials. Robert E. Kreiger; New York: 1973.

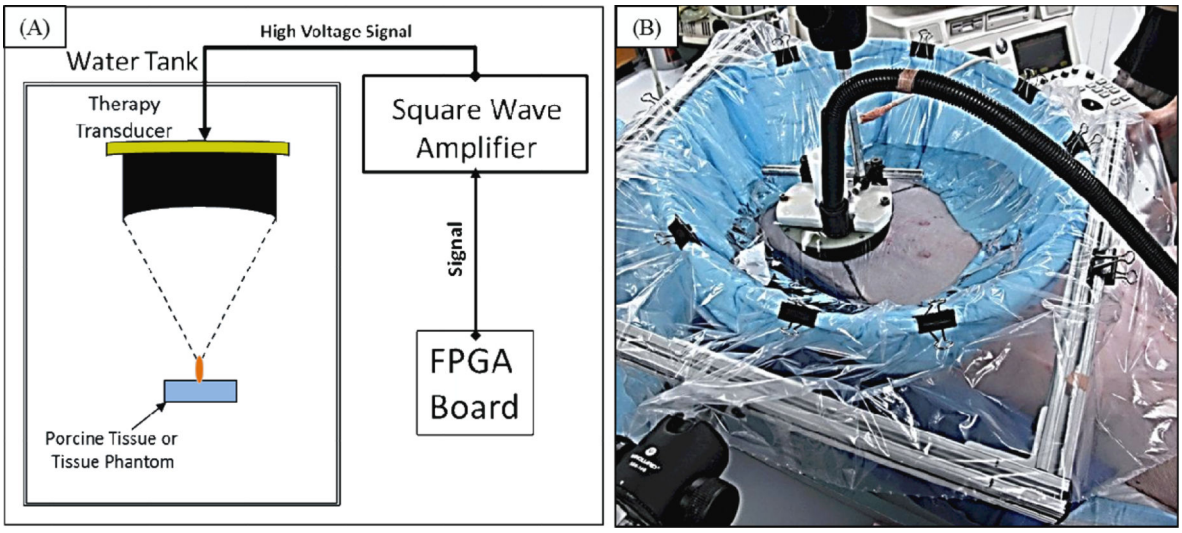

Figure 1. Experimental setups

(A) The 1 MHz therapy transducer was attached to a motorized 3D positioning system controlled using a PC console. The therapy focus was aligned at the surface of the agarose tissue phantoms and *ex vivo* porcine tissue. **(B)** For the selective ablation *in vivo* porcine experiment, an ultrasound imaging probe was coaxially mounted with the therapy transducer and the unit was attached to a motorized positioning system and coupled to the pig with a degassed water bolus.

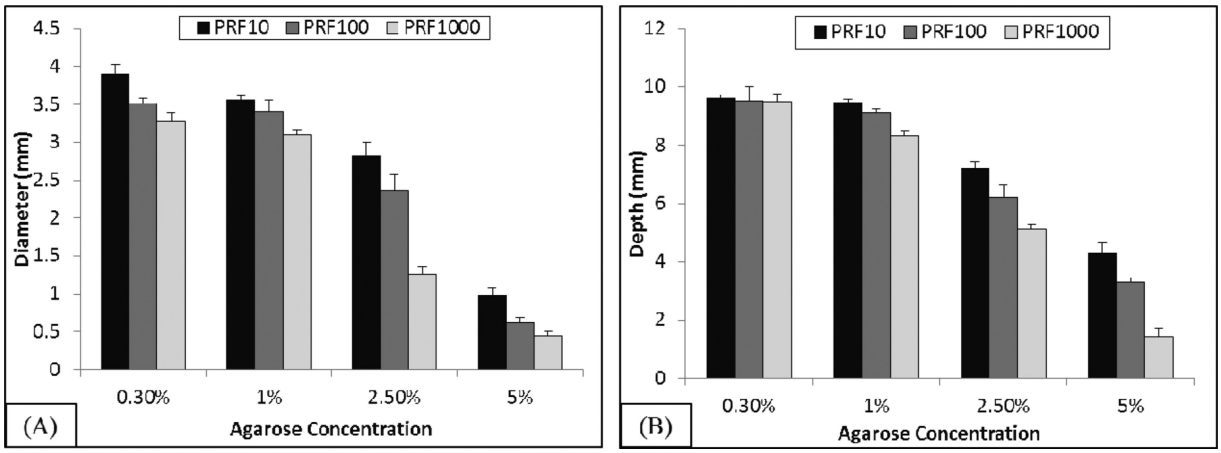

Figure 2. Histotripsy erosion lesion size decreases in higher strength agarose tissue phantoms

Tissue phantom erosion results show lesion maximum diameter **(A)** and depth **(B)** for 0.3%, 1%, 2.5%, and 5% agarose gels treated with 5,000 histotripsy pulses at 10, 100, and 1000 Hz PRF. Results show a statistically significant decrease in lesion diameter and depth with increasing agarose concentration. All observed decreases in lesion depth and diameter were considered significant ($p<0.05$) except between 0.3% and 1% agarose at 100 Hz PRF (depth: 9.52 mm, 9.1 mm, $p=0.08$; diameter: 3.52 mm, 3.41 mm, $p=0.12$). Additionally, results show a statistically significant decrease in lesion size for increased PRF.

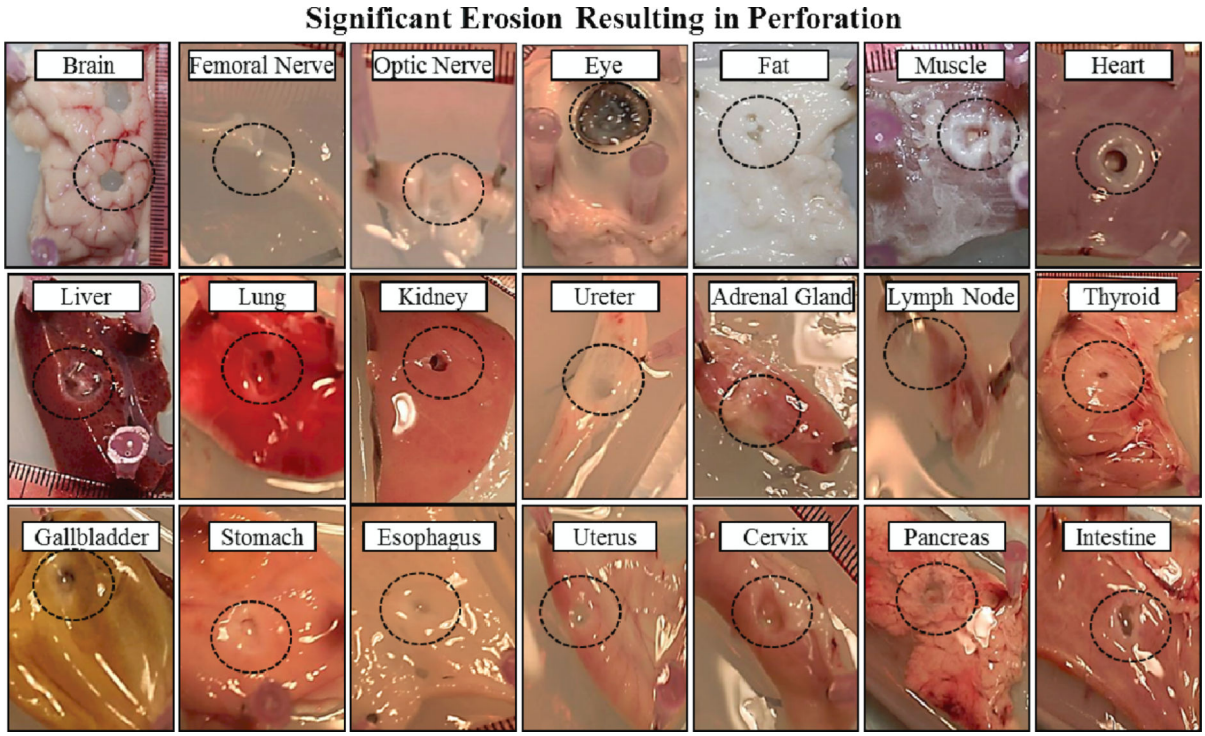

Figure 3. Histotripsy tissue erosion is capable of perforating the majority of soft tissues

Results show select images of porcine tissues treated for 10 minutes with a 1 MHz therapy transducer (1 kHz PRF, 5 cycles). Histotripsy was demonstrated to be capable of completely eroding through the majority of the soft tissues tested in this study. A complete list of *ex vivo* tissue erosion results is shown in Table 1.

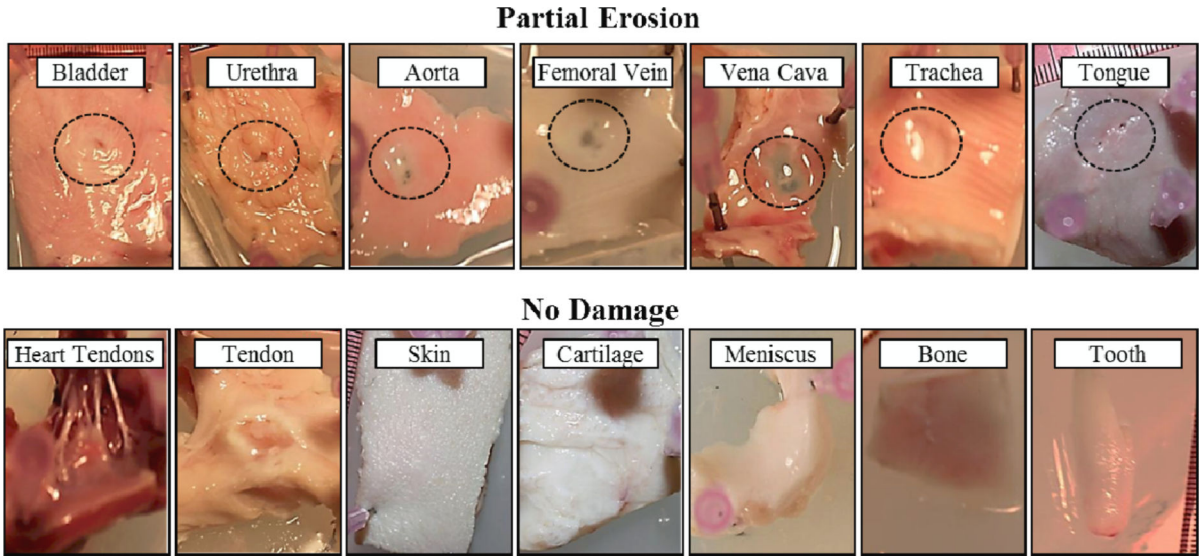

Figure 4. Histotripsy tissue erosion is less effective in tissues with increased mechanical strength

Results show selected images of porcine tissues treated for 10 minutes with a 1 MHz therapy transducer (1 kHz PRF, 5 cycles). Histotripsy treatment was demonstrated to be less effective in stronger tissues with only partial erosion or no visible damage observed. Partial erosion was most pronounced in composite tissues in which stronger layers were preserved while the weaker tissue was completely eroded (i.e. adventitial layer of vessels or cartilage layer of trachea preserved). The complete list of *ex vivo* tissue erosion results is shown in Table 1.

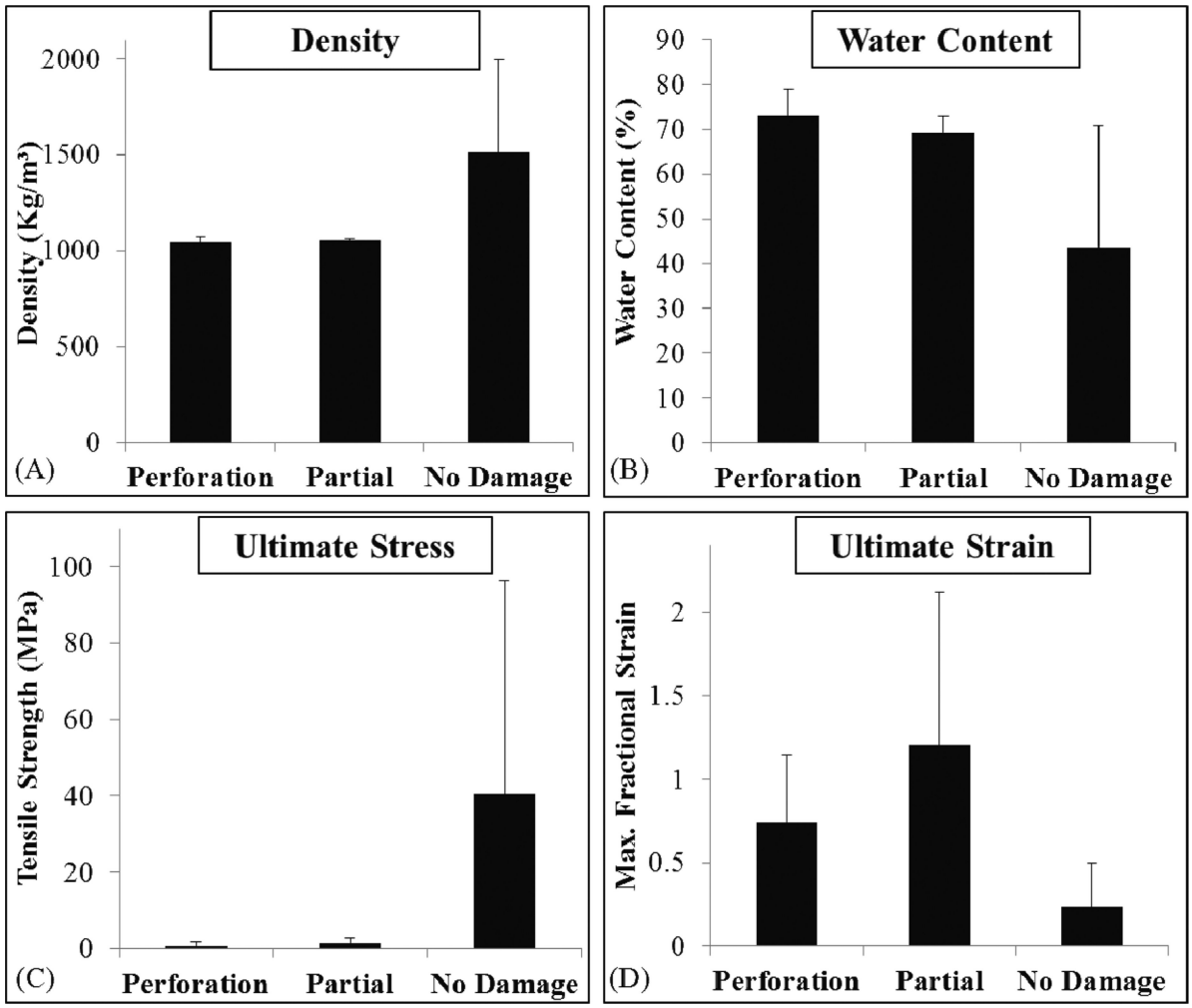

Figure 5. Comparison of selected tissue properties for histotripsy treated porcine tissues

Graphs show the average density **(A)**, water content **(B)**, tensile stress **(C)**, and ultimate fractional strain **(D)** for perforated tissues compared to tissues with partial or no damage. Undamaged tissues demonstrated statistically significantly increased density, decreased water content, increased ultimate stress, and decreased ultimate strain compared to perforated group. No statistically significant difference was observed between perforated and partial ablation groups. P-values <0.05 were considered significant.

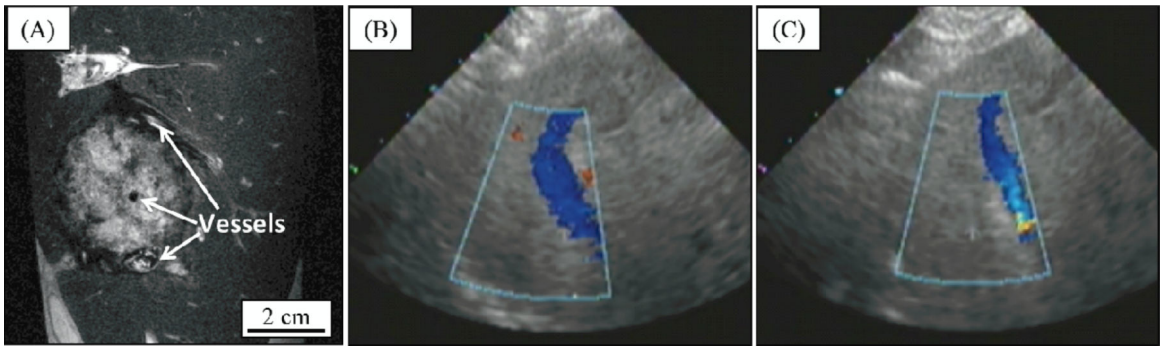

Figure 6. Histotripsy selective ablation results demonstrated large hepatic vessels remained intact and functional inside histotripsy treated porcine liver *in vivo*

Results show **(A)** MRI image of a large in vivo porcine liver histotripsy lesion with major hepatic vessels remaining structurally intact inside the completely fractionated liver tissue. Doppler ultrasound images before **(B)** and after **(C)** histotripsy treatment demonstrated large blood vessels within the treated region remained functional after histotripsy.

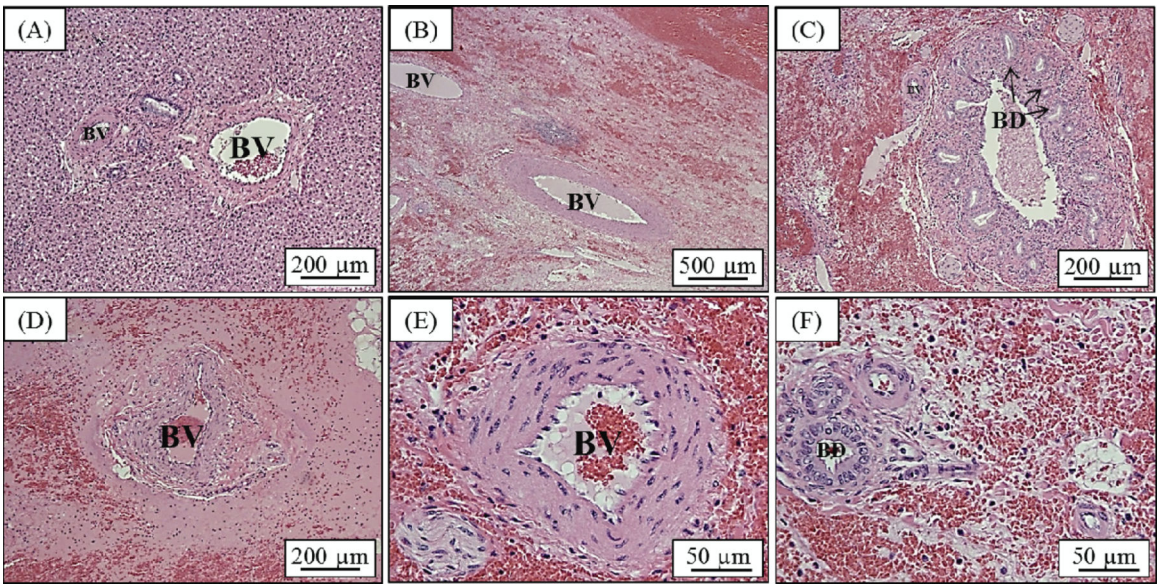

Figure 7. Histotripsy selective ablation results showed hepatic vessels remained intact within fractionated porcine liver *in vivo*

Results show select images of hepatic blood vessels (BV) inside untreated **(A)** and completely fractionated **(B-F)** liver tissue. A large number of smaller vessels and bile ducts (BD) were observed in the regions containing connective tissue surrounding hepatic vessels.

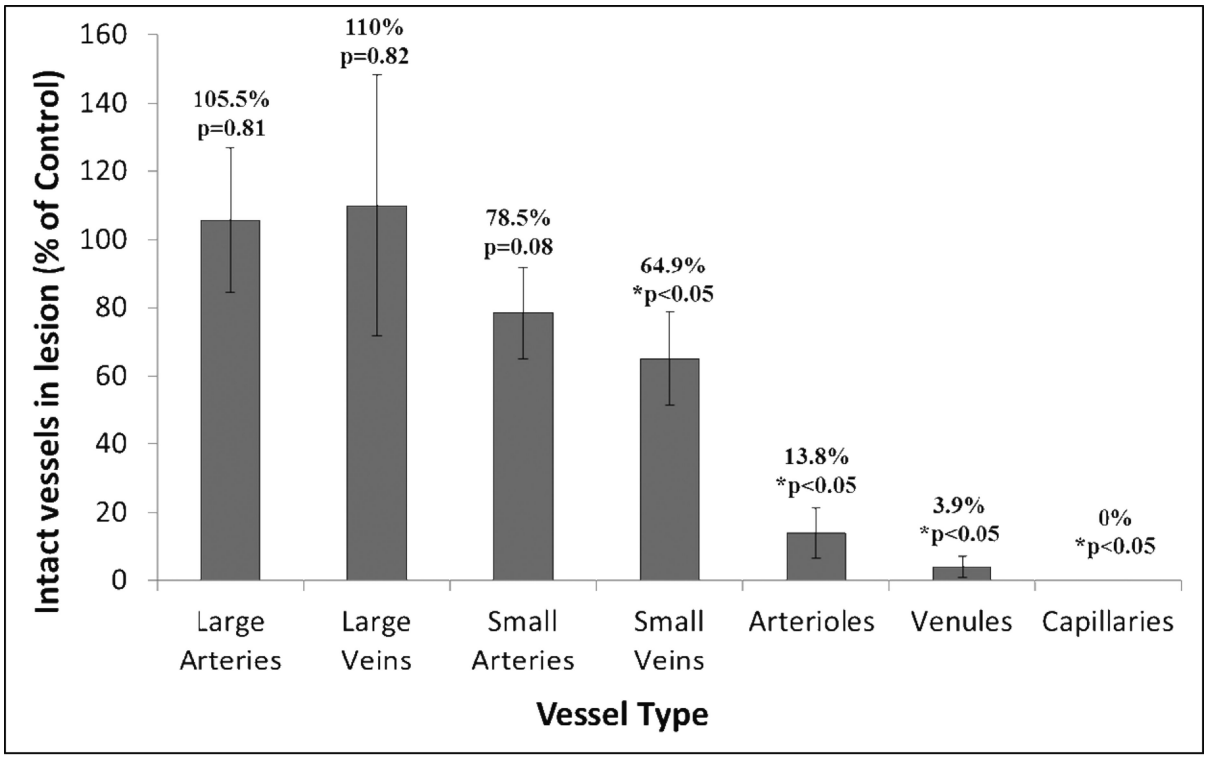

Vessel Type		Large Arteries	Large Veins	Small Arteries	Small Veins	Arterioles	Venules	Capillaries
Inner Diameter		>1 mm	>1 mm	0.3-1 mm	0.1-1 mm	20-300 μm	20-100 μm	<10 μm
Total Wall Thickness		500-1000 μm	100-500 μm	50-500 μm	10-200 μm	5-50 μm	1-20 μm	0.5 μm
Approximate Layer Thickness	Intima	0.5 μm	0.5 μm	0.5 μm	0.5 μm	0.5 μm	0.5 μm	0.5 μm
	Media	300-600 μm	40-200 μm	30-300 μm	4-80 μm	3-30 μm	0.5-8 μm	0 μm
	Adventitia	200-400 μm	60-300 μm	20-200 μm	6-120 μm	2-20 μm	0.5-12 μm	0 μm

Figure 8. Histotripsy selective ablation showed preservation of hepatic vessels was highly dependent on vessel type

(A) Plot shows the percentage of vessels remaining inside an *in vivo* porcine liver lesion formed by histotripsy organized by vessel type **(B)**. *Results showed a statistically significant decrease in small veins, arterioles, venules, and capillaries inside the histotripsy lesion compared to untreated controls ($p<0.05$).

Phys Med Biol. Author manuscript; available in PMC 2016 June 01.

Table 1

***Ex vivo* porcine tissue erosion**

The table shows complete erosion results of *ex vivo* porcine tissues treated with a 1 MHz therapy transducer for 10 minutes at a PRF of 1000 Hz and 5 cycles showing extent of the observed erosion.

Tissue	Perforation	Partial	No Erosion	Fluid Uptake	Tissue	Perforation	Partial	No Erosion	Fluid Uptake
Brain	x				Lymph node	x			
Heart	x				Ureter	x			
Fat	x				Urethra (female), inner	x			
Skeletal Muscle	x				Ovary, wall	x			
Ligament	x				Ovarian Cyst	x			
Aorta (Outside), Media	x				Uterus, wall	x			
Aorta (Outside), intima	x				Cervix	x			
Aorta (Inside), Media	x				Large Intestine	x			x
Aorta (Inside), intima	x				Small intestine	x			x
Artery, Femoral (Outside), Media	x				Thyroid	x			x
Artery, Femoral (Outside), Intima	x				Gallbladder	x			x
Artery, Femoral (Inside), Media	x				Pancreas	x			x
Artery, Femoral (Inside), Intima	x				Tongue		x		
Upper Vena Cava (Outside), Media	x				Aorta (Outside), Adventitia		x		
Upper Vena Cava (Outside), Intima	x				Aorta (Inside), Adventitia		x		
Upper Vena Cava (Inside), Media	x				Upper Vena Cava (Outside), Adventitia		x		
Upper Vena Cava (Inside), Intima	x				Upper Vena Cava (Inside), Adventitia		x		
Vein, Femoral (Outside), Media	x				Bladder		x		
Vein, Femoral (Outside), Intima	x				Skin			x	
Vein, Femoral (Outside), Media	x				Cartilage, Articular			x	
Vein, Femoral (Outside), Intima	x				Cartilage, Meniscus			x	
Liver	x				Cartilage, Elastic			x	
Eve (cavitation on surface of eye)	x				Tendon			x	
Optic Nerve	x				Artery, Femoral (Outside), Adventitia			x	
Nerve, Femoral	x				Artery, Femoral (Inside), Adventitia			x	

Tissue	Perforation	Partial	No Erosion	Fluid Uptake	Tissue	Perforation	Partial	No Erosion	Fluid Uptake
Trachea, internal lining	x				Vein, Femoral (Outside), Adventitia			x	
Lung	x				Vein, Femoral (Outside), Adventitia			x	
Esophagus	x				Heart Valve Tendons			x	
Stomach wall	x				Trachea, Cartilage			x	
Kidney, Cortex	x				Urethra (female), outer			x	
Kidney, Medulla	x				Bone, cortical			x	
Adrenal Glands	x				Bone, trabecular			x	
Spleen	x				Tooth			x	

Phys Med Biol. Author manuscript; available in PMC 2016 June 01.

Table 2

***Ex vivo* porcine tissue erosion with select tissue properties**

The table shows select results of *ex vivo* erosion in porcine tissue along with corresponding density, water content, ultimate stress, and ultimate strain values.

Tissue	Perforation	Partial	No Erosion	Fluid Uptake	Density, kg/m^3	Water Content (%)	Average ultimate tensile strength, MPa	Maximum fractional strain
Fat	x				916	21.2		
Adrenal Glands	x				1024.5	58.1		
Brain	x				1039	77.4		
Esophaaus	x				1040	76	0.59	0.73
Bladder		x			1040	65	0.24	2.26
Large Intestine	x			x	1044	79	0.68	1.17
Small intestine	x			x	1044	79	0.55	0.43
Pancreas	x			x	1045	71		
Skeletal Muscle	x				1047	74.1	0.11	0.61
Ovary, wall	x				1048	83		
Kidney	x				1049	76.6	0.05	0.52
Stomach wall	x				1050	75	0.55	0.93
Thyroid	x			x	1051	85		
Uterus, wall	x				1052	79	0.18	1.5
Spleen	x				1054	77		
Vein, Femoral		x			1056	72.6	2.9	0.66
Heart	x				1060	75.9	0.11	0.64
Liver	x				1060	74.2	0.27	0.54
Artery, Femoral		x			1062.5	70	1.4	0.69
Lung	x				1066	77.9		
Trachea, Cartilage			x		1080	60	2.4	0.19
Cartilage			x		1098	72	2.8	0.18
Skin			x		1150	65.35	11	0.685
Tendon			x		1165	63	53	0.09
Bone, trabecular			x		1920	23		

Tissue	Perforation	Partial	No Erosion	Fluid Uptake	Density, kg/m^3	Water Content (%)	Average ultimate tensile strength, MPa	Maximum fractional strain
Bone, cortical			x		1990	13.5	133	0.029
Tooth			x		2165	9.15		